Published in final edited form as:
*Cancer Res*. 2010 June 1; 70(11): 4499–4508. doi:10.1158/0008-5472.CAN-09-4264.

# Tyrosine kinase inhibitor gefitinib enhances topotecan penetration of gliomas

**Angel M. Carcaboso**[1], **Mohamed A. Elmeliegy**[1,2], **Jun Shen**[1,2], **Stephen J. Juel**[1], **Ziwei M. Zhang**[3], **Christopher Calabrese**[3], **Lorraine Tracey**[4], **Christopher M. Waters**[5], and **Clinton F. Stewart**[1,2]

[1]Department of Pharmaceutical Sciences, St. Jude Children's Research Hospital, Memphis, Tennessee

[2]Integrated Program in Biomedical Sciences, University of Tennessee Health Science Center, Memphis, Tennessee

[3]Department of Animal Imaging Core Resource, St. Jude Children's Research Hospital, Memphis, Tennessee

[4]Department of Surgery, St. Jude Children's Research Hospital, Memphis, Tennessee

[5]Department of Physiology, University of Tennessee Health Science Center, Memphis, Tennessee

## Abstract

Gefitinib, an epidermal growth factor receptor tyrosine kinase inhibitor, increases brain parenchymal extracellular fluid (ECF) accumulation of topotecan, a substrate of the ABC transporters P-glycoprotein (Pgp/MDR-1) and breast cancer resistance protein (BCRP/ABCG2). The effect of modulating these transporters on topotecan penetration in gliomas has not been thoroughly studied. Thus, we performed intracerebral microdialysis on mice bearing orthotopic human gliomas (U87 and MT330), and assessed topotecan tumor ECF (tECF) penetration and the effect of gefitinib on topotecan tECF penetration and intratumor topotecan distribution. We found that topotecan penetration ($P_{tumor}$) of U87 was 0.96 ± 0.25, n=7, compared with that of contralateral brain ($P_{contralateral}$, 0.42 ± 0.11, n=5; P = 0.001). In MT330 tumors, $P_{tumor}$ (0.78 ± 0.26, n=6) and $P_{contralateral}$ (0.42 ± 0.11, n=5) also differed significantly (P = 0.013). Since both tumor models had disrupted blood brain barriers and similar $P_{tumor}$ values, we used U87 and a steady-state drug administration approach to characterize the effect of gefitinib on topotecan $P_{tumor}$. At equivalent plasma topotecan exposures, we found that $P_{tumor}$ after gefitinib administration was lower. In a separate cohort of animals, we determined the volume of distribution of unbound topotecan in tumor ($V_{u,tumor}$) and found it was significantly higher in groups receiving gefitinib, implying that gefitinib administration leads to a greater proportion of intracellular topotecan. Our results provide crucial insights into the role that transporters play in CNS drug penetration and provide a better understanding of the effect of coadministration of transporter modulators on anticancer drug distribution within a tumor.

### Keywords

Blood brain barrier; glioma; gefitinib; microdialysis; pharmacokinetics; topotecan; drug penetration in central nervous system

Address for correspondence and reprints: Clinton F. Stewart, Pharm.D., Department of Pharmaceutical Sciences, St. Jude Children's Research Hospital, 262 Danny Thomas Place, Memphis, TN 38105-2794, Telephone: (901) 595-3665; FAX: (901) 525-6869; clinton.stewart@stjude.org.

## Introduction

Most central nervous system (CNS) tumors, particularly gliomas, are resistant to chemotherapy (1). Drug resistance in brain tumors is not well understood but may involve poor tumor-cell exposure (2), which can be caused by several mechanisms. One important mechanism involves active drug efflux from the endothelial cells forming the blood-brain barrier (BBB) by specific ATP-binding cassette (ABC) transporters (3). The irregular distribution of tumor vessels, the absence of lymphatics, and high oncotic pressure can also impede drug penetration to tumor cells distant from vessels (2). Further, some tumor cells can actively export xenobiotics via ABC transporters at the cell membrane (4). Intracellular drug exposure is crucial to the effectiveness of agents such as methotrexate (antimetabolite), paclitaxel (tubulin inhibitor), and the camptothecins (topoisomerase I inhibitors), to which cells overexpressing specific ABC transporters acquire resistance (5-7).

The semi-synthetic camptothecin analog topotecan is active against xenografted human CNS tumors (8,9) but shows little efficacy against high-grade gliomas in clinical trials (10). Poor drug penetration may contribute to this outcome. We and others observed that topotecan penetration of brain parenchyma is restricted by at least two ABC transporters, breast cancer resistance protein (BCRP/ABCG2) and P-glycoprotein (Pgp/MDR1/ABCB1) (11,12). Further, we found that the tyrosine kinase inhibitor (TKI) gefitinib increased topotecan penetration into the brain extracellular fluid (ECF) (11,13). Gefitinib, an epidermal growth factor receptor (EGFR) inhibitor, also increased the bioavailability of oral irinotecan in mice (14) and humans (15) and reversed tumor-cell resistance to topotecan and irinotecan (7,16), likely via inhibition of BCRP and Pgp (6,7). Several other TKIs are modulators of ABC transporters and have been studied, in combination with transporter-substrate chemotherapy agents, to overcome tumor drug resistance or to increase drug bioavailability (17-20).

The effect of ABC transporter inhibition on drug penetration of orthotopic brain tumor models is unknown. The BBB remains functionally intact at the margins of invasive brain tumors, where malignant cells migrate through vessel co-option to adjacent tissues (21,22); therefore, inhibitors of active drug efflux at the BBB may increase drug concentration in the tumor ECF (tECF; Ref. (11)). Efflux transporters have also been found in the neovasculature of the glioma tumor bulk (23,24). However, because tumor-secreted angiogenic molecules (e.g., vascular endothelial growth factor, VEGF) increase the permeability of vessels within the tumor bulk (25), it is unclear whether the activity of efflux transporters (and their inhibitors) is significant in these hyper-permeable tumor regions. Finally, if the tumor itself expresses ABC transporters, an inhibitor could act at the tumor-cell level to increase topotecan intracellular penetration. Here we used a combined microdialysis–tumor homogenate technique to compare the distribution of topotecan in the tECF and cells of orthotopic glioma xenografts in the presence vs. absence of the pump inhibitor gefitinib. We hypothesized that gefitinib would increase intracellular drug accumulation in ABC transporter-expressing tumors with a permeable blood-brain barrier by modulating cellular drug efflux.

## Materials and Methods

### Tumor lines

Two human glioma cell lines were used: U-87 MG (U87) and MT330. The U87 model has been extensively described (26). MT330 was created from a WHO grade IV glioma sample obtained from a patient at University Methodist Hospital (Memphis, TN) as part of an IRB-approved protocol. Both tumor lines, modified to stably express firefly luciferase (27), were donated by Dr. Andrew Davidoff (St. Jude).

### Orthotopic tumor xenografts

Animal procedures were approved by the St. Jude Animal Care and Use Committee. CD1 athymic nude mice 8–12 weeks old (Charles River Laboratories, Wilmington, MA) were anesthetized with 100 mg/kg ketamine and 10 mg/kg xylazine, and injected with $5\times10^5$ U87 or MT330 cells suspended in 5 μL Matrigel (Becton Dickinson, Bedford, MA). With the guidance of a mouse brain atlas (28), cells were injected stereotactically (David Kopf Instruments, Tujunga, CA) into the right caudate putamen.

Tumor growth was monitored by bioluminescence (IVIS-100 imaging system, Xenogen, Alameda, CA; Ref. (29)). Briefly, mice were injected intraperitoneally with 120 mg/kg D-luciferin firefly (potassium salt) (Caliper Lifesciences, Hopkinton, MA) and imaged under isoflurane anesthesia after 5 minutes. Tumor vascular permeability was assessed by contrast-enhanced magnetic resonance imaging (CE-MRI) (See Supplemental data for details).

### Topotecan penetration of tumor extracellular fluid

The concentration-time profiles of unbound drugs in tissue ECF can be characterized by microdialysis sampling coupled with an analytical method (30). We used this technique to measure the penetration of unbound topotecan lactone into tumor or brain ECF after a single intravenous (i.v.) injection of topotecan, as previously described (31). Briefly, a microdialysis guide cannula (MD-2255, Bioanalytical Systems, West Lafayette, IN) was stereotactically implanted on the day of tumor injection, either at the tumor coordinates or in the corresponding contralateral brain area. An additional group was cannulated but not inoculated with tumor. Cannulae were attached to the skull surface with dental cement and two screw anchors (MF-5182, Bioanalytical Systems). Microdialysis experiments were performed 14 to 21 days (U87) or 45 to 65 days (MT330) after tumor implantation in animals whose intracranial bioluminescence signal was at least $10^8$ photons per second or (in control animals) at least 3 days after implantation of the cannula. On the day of the experiment, a microdialysis probe (MBR-1-5, Bioanalytical Systems) was inserted through the cannula, artificial cerebrospinal fluid (aCSF; Ref. (31)) was perfused at 0.5 μL/min, and the probe membrane was allowed to equilibrate for 1 h. Topotecan (4 mg/kg) was then administered, and dialysate samples were collected every 18 min. Samples were analyzed for topotecan lactone and carboxylate with an automated microbore HPLC-fluorescence detection system until concentrations were unmeasurable (31). Probe recovery was calculated by retrodialysis as previously described (31). Using a previously described limited sampling strategy (13), we bled each mouse from the retro-orbital plexus 15, 60, and 180 min after the i.v. injection to assay plasma topotecan lactone. The unbound plasma topotecan concentration was calculated on the basis of a previous study (13), showing a 27% unbound fraction in CD1 nude mice. Unbound plasma topotecan levels were modeled by maximum *a posteriori* probability (MAP) Bayesian estimation with ADAPT 5 software (Biomedical Simulations Resource, Los Angeles, CA) (32). The prior parameter distribution was calculated by nonlinear mixed-effects modeling (NONMEM version VI; Ref (33)) in an independent group of mice receiving the same topotecan dose, as previously described (11).

The simulated concentration-time data from the ADAPT 5 model estimates were integrated to obtain the area under the concentration-time curve defining plasma exposure to unbound topotecan lactone ($AUC_{u,plasma}$). Similarly, unbound drug exposure in the dialyzed tissue (brain or tumor) ECF ($AUC_{u,tissueECF}$) was determined in each mouse (after correcting for probe recovery as previously described (31)) by three-compartment analysis of combined plasma and tissue topotecan lactone pharmacokinetic data (11). Finally, the extent of penetration of the targeted tissue by unbound topotecan lactone ($P_{tissue}$) was calculated as the tissue (*brain* or *tumor*) ECF-to-plasma AUC ratio (34):

$$P_{tissue} = \frac{AUC_{u,tissueECF}}{AUC_{u,plasma}}$$

The probe location was confirmed histologically at the end of all microdialysis experiments. In studies targeting tumor tissue, animals that had the probe outside the tumor were excluded from the analysis.

### Western blots and immunohistochemistry for ABC transporters

Western blots of U87, MT330, and control cell lysates (Saos-2-BCRP, LLC-PK1-MDR1, LS180-MRP1 and Saos-2-MRP4, stably transfected with BCRP, Pgp, MRP1, and MRP4, respectively), were performed following previously published methods (35). Membranes were incubated with 1:400 anti-BCRP (Bxp-21, Kamiya Biomedical, Seattle, WA), 1:400 anti-Pgp (C219), 1:1000 anti-MRP1 (MRPr1), or 1:1000 anti-MRP4 ($M_4$I-10; all from Alexis Biochemicals, San Diego, CA).

For immunohistochemistry, the antibodies Bxp-21 (0.5 μg/mL), JSB-1 (anti-Pgp; 1 μg/mL; Millipore Corporation, Billerica, MA), MRPr1 (2 μg/mL) and $M_4$I-10 (3 μg/ml) were used according to published protocols (13). Mouse IgG and rat IgG2a were used as negative controls.

### Effect of gefitinib on topotecan tumor extracellular fluid penetration

We maintained a constant (steady-state) topotecan concentration in plasma ($C_{ss,plasma}$) to evaluate the real-time effect of a single oral dose of gefitinib (200 mg/kg) on the topotecan tECF penetration. A topotecan-loaded mini-osmotic pump (Alzet, Model 2001D; Durect, Palo Alto, CA) was subcutaneously implanted in the CD1 nude mice; its ability to maintain a 100-ng/mL plasma topotecan lactone concentration for 24 hours had been confirmed in a group of five wild-type FVB mice (data not shown). To achieve a plasma topotecan lactone $C_{ss}$ > 100 ng/mL (bound + unbound) in U87 tumor-bearing mice, we loaded the pump with 4 mg/mL topotecan in sterile water, which was released at 25 μg/h for 24 hours.

For microdialysis studies, the probe recovery was calculated by retrodialysis prior to the pharmacokinetic experiment. Then, the probe was washed by perfusion for 1 h with aCSF at 2 μL/min. Mice were then anesthetized with isoflurane, a topotecan-loaded pump previously primed in 0.9% saline (3 hours, 37°C) was surgically inserted under the skin of the back, and the incision was sutured. The aCSF flow rate was then reduced to 0.5 μL/min and dialysate samples were collected overnight every 18 min, as described above. The next morning (12-14 h after pump insertion), a plasma sample was obtained to characterize unbound $C_{ss,plasma}$ and a 200 mg/kg gefitinib dose was administered orally as previously described (13). Dialysate sample collection and analysis continued for 8-10 hours and plasma samples were obtained retroorbitally 4, 6, and 8 hours after gefitinib administration. The $C_{ss}$ of unbound topotecan lactone in tECF ($C_{ss,tECF}$) was calculated before (mean concentration of dialysate samples collected 6 h to 14 h post–pump insertion) and after (mean concentration of dialysate samples collected 6 h to 8 h after gefitinib) the gefitinib dose. The steady-state penetration of tECF ($P_{tumor}$) by unbound topotecan lactone was calculated as the $C_{ss,tECF}/C_{ss,plasma}$ ratio (34).

### Intratumor distribution of topotecan

To determine the proportion of drug either entrapped in the intracellular compartment or nonspecifically bound to tumor tissue components, in relation to the unbound drug fraction in the tECF, we applied the “unbound drug volume of distribution in tumor” ($V_{u,tumor}$) parameter, adapted from Wang and Welty (36). $V_{u,tumor}$ describes the relationship, at the steady-state, between the total drug concentration in the tumor (assayed in homogenized tissue) and the

unbound drug concentration in tECF (calculated by microdialysis). $V_{u,tumor}$ is measured in mL/g tumor:

$$V_{u,tumor} = \frac{A_{tot,tumor} - V_{tot,blood} \times C_{tot,blood}}{C_{ss,tECF}}$$

where $A_{tot,tumor}$ is the total quantity of drug per gram of tumor homogenate (including blood present in the tumor), $V_{blood}$ is the volume of blood per gram of tumor, $C_{tot,blood}$ is the total concentration of drug in blood, and $C_{ss,tECF}$ is the measured concentration of unbound drug in the tECF.

We obtained experimental $A_{tot,tumor}$ and $C_{tot,blood}$ data by performing studies in additional groups of mice bearing U87 tumors, using timing similar to that described above. One group, TPT25 (n=8), received pump-infused topotecan at a constant rate of 25 μg/h. These animals were sacrificed 8-12 h after insertion of the pump (at steady-state) and blood and tumor tissues were harvested for HPLC drug assays, performed as already published (37). The effect of gefitinib on the $V_{u,tumor}$ parameter was assessed in two additional groups of U87 tumor–bearing mice. The TPT25-GEF group (n=7) received topotecan at 25 μg/h and received oral gefitinib (200 mg/kg) 8 hours before sacrifice. The TPT12-GEF group (n=6) received an adjusted dose of topotecan (12.5 μg/h) to achieve systemic exposure ($C_{ss,plasma}$) comparable to that in the TPT25 group and received oral gefitinib (200 mg/kg) 8 hours before sacrifice. Tumors were immediately frozen and stored at -80°C. For drug analysis, tumors were weighed and homogenized ultrasonically (CP-50, Cole-Parmer, Chicago, IL) at 4°C in water (10 μL/mg of tumor). The tumor suspension (200 μL) was mixed with 800 μL of cold methanol, mixed vigorously, and centrifuged for 10 min at 14,000 rpm at 4°C. The supernatant was filtered in Spin-X Centrifuge filter tubes (Costar, Cambridge, MA) at 14,000 rpm at 4°C for 10 minutes. Filtrates were stored at -80°C for HPLC assay.

To estimate the $V_{u,tumor}$ parameter in the TPT25 and TPT25-GEF groups, we used the mean $C_{ss,tECF}$ values obtained in the previous steady-state microdialysis experiments. The value $V_{blood}$ for intracranial U87 tumors in mice was obtained from the literature (4.1% (38)). In the TPT12-GEF group we performed a new set of microdialysis experiments (n=3) to obtain the $C_{ss,tECF}$ value (as described above) in animals bearing U87 tumors and colocalized microdialysis cannulae; in this group, gefitinib (200 mg/kg, oral) was administered 30 min before insertion of a pump dispensing 12.5 μg/h of topotecan. Dialysate samples were collected 8-10 hours after insertion and a blood sample was obtained 8 hours after gefitinib administration.

### Intracellular accumulation of topotecan in vitro

Cells ($5\times10^5$ per well in 2 mL medium) were incubated overnight in 6-well tissue culture plates (Becton Dickinson), and 2 mL of medium containing topotecan (final concentration, 1 μM) with or without gefitinib (final concentration, 10 μM) was then added. After incubation at 37°C for 1, 5 or 10 minutes, the medium was rapidly aspirated to terminate drug accumulation, and the wells were washed with ice-cold PBS (2×5 mL). Ice-cold water was added (500 μL/well), and cell suspensions were transferred to microcentrifuge tubes on ice. Samples were suspended ultrasonically, and 100 μL of suspension was added to 400 μL of cold methanol. The mixture was mixed vigorously and centrifuged for 10 min at 14,000 rpm at 4°C. The supernatant was filtered in a Costar Spin-X Centrifuge filter tube at 14,000 rpm at 4°C for 3 minutes. Filtrates were stored at -80°C for HPLC assay. Samples were analyzed by HPLC as described previously (31).

### Drug sensitivity

The antitumor activity of topotecan, gefitinib, and their combinations was determined *in vitro* in U87 and MT330 tumor models as previously described (6). After 4 hour incubation, the drug-containing medium was replaced with fresh medium and the proportion of viable cells was determined 4 days later.

### Statistics

Aggregate data are presented as mean ± SD. Paired *t* test was used to compare variables in animals before and after a treatment (i.e., gefitinib). Student's *t* test and the Mann-Whitney test (for non–normally distributed data) were used for non-paired comparisons of two groups. For the comparison of more than two groups, a one-way ANOVA was performed followed by a post-hoc *t* test with Bonferroni correction.

## Results

### Glioma morphology and growth in vivo

We studied drug penetration of gliomas by orthotopically implanting the most frequently used glioma cell line (U87) and a new, low-passage primary tumor line (MT330). The tumor cells engrafted in 100% (58/58, U87) and 85% (17/19, MT330) of inoculated animals. U87 tumors, as previously described (39), were round and non-infiltrative (Figure 1A), had profuse, uniform vascularization, and were easily dissected from surrounding brain under a dissecting microscope. In contrast, MT330 tumors infiltrated contiguous brain parenchyma, had irregular edges, had inhomogeneous core vasculature, and could be dissected only by using a bioluminescence-guided technique.

Tumor growth, as measured by increased bioluminescence signal (29), was also dissimilar (Figure 1B): U87 tumors were larger than 50 $mm^3$ (assessed by terminal dissection) 2 to 3 weeks after implantation, and most animals showed neurologic signs (altered balance, lethargy) within 3 weeks. MT330 tumors grew slowly for several weeks before reaching the luminescence intensity and tumor volume (47 ± 14 $mm^3$ as assessed by MRI—as specified in Supplemental Data—at week 15; n = 5 mice) of U87 tumors.

### Permeability of the tumor vasculature

We chose to characterize the BBB of our tumor models using a contrast-enhanced MRI approach. If the BBB were disrupted, CNS drug penetration would be altered and it would be possible to assess the effect of ABC transporter inhibitors at the level of tumor cells (not tumor vessel). Using CE-MRI we characterized the vascular integrity of both U87 and MT330, and images showed significant contrast enhancement, which confirmed an impaired BBB (Supplemental Figure 1A). Homogeneous enhancement was observed in U87 tumors, significantly greater than enhancement in the contralateral brain tissue (Supplemental Figure 1B). Contrast in MT330 tumors was inhomogeneous, with areas of high signal intensity which may have indicated heavy vascularization and/or necrosis.

### Topotecan penetration of tumor extracellular fluid

We anticipated greater drug concentrations within U87 and MT330 tECF than in normal brain tissue ECF because of the tumors' greater vascular permeability. Our previous microdialysis studies showed the exposure of brain ECF to unbound topotecan lactone to be 21%-36% that of plasma after a 4 mg/kg i.v. bolus injection in FVB mice (11,13). Here, using an identical experimental setup, we first evaluated brain ECF penetration in non-tumor-bearing CD1 nude mice; results were within the range previously reported ($P_{brain}$ = 0.30 ± 0.11, n=7). We then compared tECF vs. contralateral brain ECF penetration in animals bearing U87 and MT330

tumors. Unbound drug penetration of U87 tECF ($P_{tumor}$ = 0.96 ± 0.25, n=7) was 2.3 times that of contralateral brain ECF ($P_{contralateral}$ = 0.42 ± 0.11, n=5; P = 0.001; *t* test) (Figure 2A). In MT330 tumors, $P_{tumor}$ (0.78 ± 0.26, n=6) and $P_{contralateral}$ (0.42 ± 0.11, n=5) also differed significantly (2.2-fold; P = 0.013; *t* test). $P_{contralateral}$ values did not differ statistically from $P_{brain}$ values in the non-tumor-bearing mice. Tumor targeting (% experiments with probe in tumor) was more accurate in the U87 model (88%) than in the MT330 model (55%). Figure 2B shows representative experiments.

## Expression of ABC transporters in tumor lines and xenografts

Because one of our objectives was to evaluate the effect of inhibition of tumor cell ABC transporters on drug penetration, we examined the presence of these transporters by western blot (in the cell lines) and immunohistochemistry (in the xenografts). As shown in Figure 3A, BCRP, MRP1, and MRP4 were present in both tumor lines, while Pgp was not detected. In the U87 and MT330 xenografts, BCRP and MRP1 were strongly expressed, and Pgp and MRP4 were expressed moderately or weakly (Figure 3B).

## Gefitinib shifts intratumor topotecan distribution toward the intracellular compartment

To describe drug distribution in the tECF, vascular, and intracellular tumor compartments, we maintained a constant plasma drug concentration, determined the $C_{ss,tECF}/C_{ss,plasma}$ ratio ($P_{tumor}$), and estimated intratumor distribution ($V_{u,tumor}$) by using combined data sets obtained from microdialysis and homogenate samples. This strategy allowed us to 1) use fewer animals than studies using i.v. injections, which require serial tissue samples; 2) characterize the real-time effects of gefitinib on topotecan pharmacokinetics; and 3) achieve equivalent systemic exposures in animal groups that did and did not receive gefitinib.

We previously showed that gefitinib (likely through its interaction with ABC transporters) halves topotecan lactone plasma clearance (11,13). In our steady-state studies, $C_{ss,plasma}$ (unbound lactone) was 34 ± 8 ng/mL (n=15) after a 25-μg/h topotecan infusion but increased to 109 ± 42 ng/mL after administration of gefitinib (n=15; P < 0.001). Figure 4A displays plasma unbound topotecan lactone concentration in all experiments in which gefitinib was administered 14 hours after topotecan pump insertion. In the TPT12-GEF group (n=6), which received 200 mg/kg gefitinib before pump insertion, we corrected the topotecan dosage to 12.5 μg/h and achieved plasma exposure ($C_{ss,plasma}$, 33 ± 2 ng/mL) similar to that in animals receiving 25 μg/mL without gefitinib.

We used the U87 model to characterize intratumor drug distribution with the steady-state approach, because these tumors are easily identified and dissected, grow faster and more consistently, and have an ABC transporter expression profile similar to that of MT330 tumors. We first performed microdialysis experiments to define topotecan $C_{ss,tECF}$. After a 25-μg/h topotecan infusion, the mean $C_{ss,tECF}$ was 22 ± 10 ng/mL (n=10); after administration of gefitinib (200 mg/kg), mean $C_{ss,tECF}$ increased to 30 ± 12 ng/mL (n=10) (P = 0.019; paired *t* test). Figure 4B shows a representative experiment in a single animal.

Microdialysis experiments were also performed in the TPT12-GEF group, which received 12.5 μg/h topotecan after 200 mg/kg gefitinib. $C_{ss,tECF}$ (6.4 ± 0.8 ng/mL, n=3) was significantly lower than that in animals that had not received gefitinib (P = 0.014, Mann-Whitney test).

When $P_{tumor}$ (i.e., $C_{ss,tECF}/C_{ss,plasma}$ ratio) was calculated, we observed lower ratios in both groups of animals receiving gefitinib than in the TPT25 group (without gefitinib) (Figure 4C). We hypothesized that gefitinib might have depleted topotecan lactone from the tECF and induced drug accumulation in the intracellular compartment, likely by inhibiting ABC transporters in the tumor cells.

To test our hypothesis, we calculated the volume of distribution of unbound drug in tumor ($V_{u,tumor}$) to describe intratumor drug distribution *in vivo*. New studies in U87 tumor-bearing mice provided the total (bound + unbound) topotecan lactone concentration at the steady-state in tumor homogenates ($A_{tot,tumor}$ 47 ± 21, 142 ± 67, and 43 ± 17 ng/mg tumor) and blood ($C_{tot,blood}$ 105 ± 33, 219 ± 81, and 109 ± 8 ng/mL) of the TPT25 (n=8), TPT25-GEF (n=7), and TPT12-GEF (n=6) groups, respectively. The mean unbound topotecan tECF concentrations ($C_{ss,tECF}$) from the microdialysis experiments were then used to calculate $V_{u,tumor}$. As shown in Figure 5A, $V_{u,tumor}$ was significantly higher in groups receiving gefitinib. Thus, after administration of gefitinib a greater proportion of drug was intracellular or nonspecifically bound to tumor tissue components rather than as unbound drug in the tECF.

To further characterize intracellular topotecan accumulation in the presence of gefitinib, we incubated U87 and MT330 cells with topotecan 0.1 μM and gefitinib 1 or 10 μM. Topotecan accumulation was enhanced as much as 36% by gefitinib in both U87 and MT330 cells, in a dose-dependent manner (Figure 5B). This finding supports the shift of topotecan distribution toward the intracellular compartment in the presence of gefitinib.

### Effect of gefitinib on tumor-cell sensitivity to topotecan

To assess whether gefitinib sensitizes tumor cells to topotecan, we measured the growth of U87 and MT330 cells in the presence of topotecan, topotecan plus gefitinib (1 or 10 μM), and gefitinib alone (Figure 6). Gefitinib alone (0.001-50 μM) did not substantially affect growth, but the $IC_{50}$ values of topotecan decreased in both cell lines with the addition of 10 μM gefitinib (U87, from 15.1 (12.3-17.8) μM to 3.54 (2.73-4.34) μM; MT330, from 4.81 (3.84-5.79) μM to 3.27 (2.71-3.83) μM; means and 95% confidence intervals are provided).

## Discussion

The ability of selected tyrosine kinase inhibitors to enhance drug penetration of tumors by inhibiting ABC transporters *in vivo* is not completely understood. Here we used two glioma models—a cell line (U87) and a primary culture (MT330)—to assess the effect of the TKI gefitinib on the tumor penetration and intratumor distribution of topotecan, both *in vitro* and in orthotopic xenografts in CD1 athymic nude mice. Our results demonstrate that the pharmacological interaction of the drugs results in increased intracellular tumor exposure to topotecan. The experimental model we used provides a novel method of assessing the effect of a modulator of drug efflux on the intratumor distribution of a chemotherapy agent in orthotopically engrafted brain tumors.

Our previous studies of topotecan-gefitinib and irinotecan-gefitinib combinations in transporter-overexpressing cells (6,14,35) and in brain penetration analyses (11,13) showed that gefitinib inhibits at least two topotecan transporters: BCRP and Pgp. The inhibition of these two transporters in brain tumors could affect drug efflux at two levels: BBB vessels and tumor cells. We previously demonstrated in an intact BBB model that gefitinib enhances drug penetration of the BBB (11,13); in the present study, we focused on its effect at the tumor-cell level. Therefore, we selected tumor models (U87 and MT330) that show increased vascular permeability (altered BBB) and ABC transporter expression. The U87 tumor vasculature does express multi-drug resistance proteins like Pgp that may act as drug efflux pumps in intracerebral tumor models (23,40). However, our contrast MRI (Supplemental Figure 1) and microdialysis (Figure 2) results, which confirm the increased permeability of the U87 tumor vessels, call into question the activity of this or other putative transporters at the tumor-vessel level. At the cellular level, we found abundant BCRP expression in U87 and MT330 lines, consistent with clinical findings in gliomas (41). Topotecan is also a substrate of MRP4 (35) and likely of MRP1 (42), both of which we found in U87 and MT330 tumor lines (Figure 3). To our knowledge, gefitinib inhibition of MRP4 and MRP1 has not been studied in detail,

although a similar compound, erlotinib, did not alter MRP1-related drug resistance (17). Therefore, the activity of MRP1 and MRP4 in our tumor lines may at least partially explain their relatively high resistance to topotecan, even in the presence of gefitinib.

The steady-state experimental approach allowed us to observe the *real-time* effects of gefitinib on the topotecan tECF-to-plasma concentration ratio in individual animals. The decrease in this ratio after gefitinib administration was confirmed in a group of gefitinib-exposed animals (*TPT12-GEF*) whose topotecan dose was reduced to achieve systemic exposure equivalent to that achieved without gefitinib at a higher dosage (25 μg/h) (equivalent plasma exposure helped to minimize the effect in which higher plasma levels can increase drug penetration of the intracellular compartment). These observations prompted us to investigate whether inhibition of transporters at the tumor-cell level would drive drug distribution toward the tumor intracellular compartment. Data from our *in vivo* studies of homogenate-microdialysis concentration and from our *in vitro* studies of intracellular accumulation supported this shift in topotecan intratumor distribution. We did not evaluate intratumor gefitinib concentration, although good penetration was reported in subcutaneous glioma xenografts (gefitinib concentration > 20 μM for 8 hours after a single oral dose of 55 mg/kg) (43). In patients with gliomas who received gefitinib (500 mg, orally for 5 days) before tumor resection, gefitinib $C_{ss}$ was 7-25 μM in the tumor homogenate (44).

We attempted the steady-state experimental approach to study the effect of gefitinib on topotecan CNS penetration in nontumor bearing mice. However, we did not obtain interpretable data from this experiment because the intact BBB limited CNS drug penetration in a way that, with our bioanalytical system, we could not detect topotecan in the ECF dialysates collected before the administration of gefitinib. A plausible reason for this limitation of the infusion approach is that slow drug infusions penetrate the intact CNS less efficiently as compared to rapid bolus injections, likely because the plasma concentration driving drug diffusion across the BBB is much lower in the case of the infusions (45). Increasing the infusion rate to achieve elevated plasma $C_{ss}$ in the nontumor bearing animals might have rendered detectable drug levels in the ECF, but the toxicity of topotecan at such increased plasma $C_{ss}$ precluded performing this study.

We suggest that microdialysis *alone* is only partially informative in brain tumor drug penetration studies, because 1) high drug concentrations in tECF would be expected, given the usually altered BBB, and 2) only drugs in the tECF are analyzed, while most chemotherapy agents have intracellular targets. Further, microdialysis measurement of drug concentration in intracranial tumors is complex (40,46,47). Microdialysis was recently used elegantly to identify very high methotrexate levels in the tECF of patients' highly contrasting gliomas, but as mentioned above, these levels do not reveal the tumor-cell penetration of the drug (46). New techniques like the one proposed by Langer et al., combining positron emission tomography (PET) and microdialysis, may overcome the limitations of microdialysis alone and allow assessment of intracellular drug penetration in unresected human tumors (48).

To conclude, ours is the first report characterizing the role of drug efflux inhibitors in shifting the intratumor distribution of substrate drugs toward the cellular compartment in an orthotopic glioma model. Specific sampling and analysis methods are necessary to assess the intratumor distribution of anticancer drugs. Future studies to bring these concepts into the preclinical and clinical fields are warranted. One example is the use of irinotecan in combination with the antiangiangiogenic agent bevacizumab for recurrent glioma (49). As prolonged antiangiogenic therapy is reportedly associated with restoration of the BBB (50), future studies should address how the possible recovery of the BBB and inhibitors of drug efflux affect the penetration of brain tumors by irinotecan.

## Supplementary Material

Refer to Web version on PubMed Central for supplementary material.

## Acknowledgments

We thank Sharon Naron for editorial assistance.

This work was supported in part by grants CA23099, CA21765, and GM071321 from the U.S. Public Health Service and by the American Lebanese Syrian Associated Charities (ALSAC).

## References

1. Wen PY, Kesari S. Malignant gliomas in adults. N Engl J Med 2008;359:492–507. [PubMed: 18669428]
2. Tredan O, Galmarini CM, Patel K, Tannock IF. Drug resistance and the solid tumor microenvironment. J Natl Cancer Inst 2007;99:1441–54. [PubMed: 17895480]
3. Loscher W, Potschka H. Drug resistance in brain diseases and the role of drug efflux transporters. Nat Rev Neurosci 2005;6:591–602. [PubMed: 16025095]
4. Gottesman MM, Fojo T, Bates SE. Multidrug resistance in cancer: role of ATP-dependent transporters. Nat Rev Cancer 2002;2:48–58. [PubMed: 11902585]
5. Maliepaard M, van Gastelen MA, de Jong LA, Pluim D, van Waardenburg RC, Ruevekamp-Helmers MC, et al. Overexpression of the BCRP/MXR/ABCP gene in a topotecan-selected ovarian tumor cell line. Cancer Res 1999;59:4559–63. [PubMed: 10493507]
6. Leggas M, Panetta JC, Zhuang Y, Schuetz JD, Johnston B, Bai F, et al. Gefitinib modulates the function of multiple ATP-binding cassette transporters in vivo. Cancer Res 2006;66:4802–7. [PubMed: 16651435]
7. Yang CH, Huang CJ, Yang CS, Chu YC, Cheng AL, Whang-Peng J, et al. Gefitinib reverses chemotherapy resistance in gefitinib-insensitive multidrug resistant cancer cells expressing ATP-binding cassette family protein. Cancer Res 2005;65:6943–9. [PubMed: 16061679]
8. Friedman HS, Houghton PJ, Schold SC, Keir S, Bigner DD. Activity of 9-dimethylaminomethyl-10-hydroxycamptothecin against pediatric and adult central nervous system tumor xenografts. Cancer Chemother Pharmacol 1994;34:171–4. [PubMed: 8194169]
9. Houghton PJ, Cheshire PJ, Hallman JD, Lutz L, Friedman HS, Danks MK, et al. Efficacy of topoisomerase I inhibitors, topotecan and irinotecan, administered at low dose levels in protracted schedules to mice bearing xenografts of human tumors. Cancer Chemother Pharmacol 1995;36:393–403. [PubMed: 7634381]
10. Chintagumpala MM, Friedman HS, Stewart CF, Kepner J, McLendon RE, Modrich PL, et al. A phase II window trial of procarbazine and topotecan in children with high-grade glioma: a report from the children's oncology group. J Neurooncol 2006;77:193–8. [PubMed: 16314955]
11. Shen J, Carcaboso AM, Hubbard KE, Tagen M, Wynn HG, Panetta JC, et al. Compartment-specific roles of ATP-binding cassette transporters define differential topotecan distribution in brain parenchyma and cerebrospinal fluid. Cancer Res 2009;69:5885–92. [PubMed: 19567673]
12. de Vries NA, Zhao J, Kroon E, Buckle T, Beijnen JH, van Tellingen O. P-glycoprotein and breast cancer resistance protein: two dominant transporters working together in limiting the brain penetration of topotecan. Clin Cancer Res 2007;13:6440–9. [PubMed: 17975156]
13. Zhuang Y, Fraga CH, Hubbard KE, Hagedorn N, Panetta JC, Waters CM, et al. Topotecan central nervous system penetration is altered by a tyrosine kinase inhibitor. Cancer Res 2006;66:11305–13. [PubMed: 17145877]
14. Stewart CF, Leggas M, Schuetz JD, Panetta JC, Cheshire PJ, Peterson J, et al. Gefitinib enhances the antitumor activity and oral bioavailability of irinotecan in mice. Cancer Res 2004;64:7491–9. [PubMed: 15492275]
15. Furman WL, Navid F, Daw NC, McCarville MB, McGregor LM, Spunt SL, et al. Tyrosine kinase inhibitor enhances the bioavailability of oral irinotecan in pediatric patients with refractory solid tumors. J Clin Oncol 2009;27:4599–604. [PubMed: 19687340]

16. Nagashima S, Soda H, Oka M, Kitazaki T, Shiozawa K, Nakamura Y, et al. BCRP/ABCG2 levels account for the resistance to topoisomerase I inhibitors and reversal effects by gefitinib in non-small cell lung cancer. Cancer Chemother Pharmacol 2006;58:594–600. [PubMed: 16520985]
17. Shi Z, Peng XX, Kim IW, Shukla S, Si QS, Robey RW, et al. Erlotinib (Tarceva, OSI-774) antagonizes ATP-binding cassette subfamily B member 1 and ATP-binding cassette subfamily G member 2-mediated drug resistance. Cancer Res 2007;67:11012–20. [PubMed: 18006847]
18. Dai CL, Tiwari AK, Wu CP, Su XD, Wang SR, Liu DG, et al. Lapatinib (Tykerb, GW572016) reverses multidrug resistance in cancer cells by inhibiting the activity of ATP-binding cassette subfamily B member 1 and G member 2. Cancer Res 2008;68:7905–14. [PubMed: 18829547]
19. Molina JR, Kaufmann SH, Reid JM, Rubin SD, Galvez-Peralta M, Friedman R, et al. Evaluation of lapatinib and topotecan combination therapy: tissue culture, murine xenograft, and phase I clinical trial data. Clin Cancer Res 2008;14:7900–8. [PubMed: 19047120]
20. Houghton PJ, Germain GS, Harwood FC, Schuetz JD, Stewart CF, Buchdunger E, et al. Imatinib mesylate is a potent inhibitor of the ABCG2 (BCRP) transporter and reverses resistance to topotecan and SN-38 in vitro. Cancer Res 2004;64:2333–7. [PubMed: 15059881]
21. Leenders WP, Kusters B, de Waal RM. Vessel co-option: how tumors obtain blood supply in the absence of sprouting angiogenesis. Endothelium 2002;9:83–7. [PubMed: 12200959]
22. Winkler F, Kienast Y, Fuhrmann M, Von Baumgarten L, Burgold S, Mitteregger G, et al. Imaging glioma cell invasion in vivo reveals mechanisms of dissemination and peritumoral angiogenesis. Glia 2009;57:1306–15. [PubMed: 19191326]
23. Fellner S, Bauer B, Miller DS, Schaffrik M, Fankhanel M, Spruss T, et al. Transport of paclitaxel (Taxol) across the blood-brain barrier in vitro and in vivo. J Clin Invest 2002;110:1309–18. [PubMed: 12417570]
24. Toth K, Vaughan MM, Peress NS, Slocum HK, Rustum YM. MDR1 P-glycoprotein is expressed by endothelial cells of newly formed capillaries in human gliomas but is not expressed in the neovasculature of other primary tumors. Am J Pathol 1996;149:853–8. [PubMed: 8780389]
25. Argaw AT, Gurfein BT, Zhang Y, Zameer A, John GR. VEGF-mediated disruption of endothelial CLN-5 promotes blood-brain barrier breakdown. Proc Natl Acad Sci U S A 2009;106:1977–82. [PubMed: 19174516]
26. Weller M, Rieger J, Grimmel C, Van Meir EG, De Tribolet N, Krajewski S, et al. Predicting chemoresistance in human malignant glioma cells: the role of molecular genetic analyses. Int J Cancer 1998;79:640–4. [PubMed: 9842975]
27. Dickson PV, Hamner B, Ng CY, Hall MM, Zhou J, Hargrove PW, et al. In vivo bioluminescence imaging for early detection and monitoring of disease progression in a murine model of neuroblastoma. J Pediatr Surg 2007;42:1172–9. [PubMed: 17618876]
28. Paxinos, G.; Franklin, KBJ. The mouse brain in stereotaxic coordinates. San Diego: Academic Press; 2001.
29. Szentirmai O, Baker CH, Lin N, Szucs S, Takahashi M, Kiryu S, et al. Noninvasive bioluminescence imaging of luciferase expressing intracranial U87 xenografts: correlation with magnetic resonance imaging determined tumor volume and longitudinal use in assessing tumor growth and antiangiogenic treatment effect. Neurosurgery 2006;58:365–72. discussion -72. [PubMed: 16462491]
30. Chefer VI, Thompson AC, Zapata A, Shippenberg TS. Overview of brain microdialysis. Curr Protoc Neurosci 2009;Chapter 7(Unit7):1. [PubMed: 19340812]
31. Leggas M, Zhuang Y, Welden J, Self Z, Waters CM, Stewart CF. Microbore HPLC method with online microdialysis for measurement of topotecan lactone and carboxylate in murine CSF. J Pharm Sci 2004;93:2284–95. [PubMed: 15295789]
32. D'argenio, DZ.; Schumitzky, A. ADAPT 5 User's Guide: Pharmacokinetic/Pharmacodynamic Systems Analysis Software. Biomedical Simulations Resource; Los Angeles: 2009.
33. Beal, SL. Introduction to version IV. Ellicott City, MD: ICON Development Solutions; 2006. NONMEM Users' Guide.
34. Hammarlund-Udenaes M, Friden M, Syvanen S, Gupta A. On the rate and extent of drug delivery to the brain. Pharm Res 2008;25:1737–50. [PubMed: 18058202]

35. Leggas M, Adachi M, Scheffer GL, Sun D, Wielinga P, Du G, et al. Mrp4 confers resistance to topotecan and protects the brain from chemotherapy. Mol Cell Biol 2004;24:7612–21. [PubMed: 15314169]
36. Wang Y, Welty DF. The simultaneous estimation of the influx and efflux blood-brain barrier permeabilities of gabapentin using a microdialysis-pharmacokinetic approach. Pharm Res 1996;13:398–403. [PubMed: 8692732]
37. Hubbard KE, Schaiquevich P, Bai F, Fraga CH, Miller L, Panetta JC, et al. Application of a highly specific and sensitive fluorescent HPLC method for topotecan lactone in whole blood. Biomed Chromatogr 2009;23:707–13. [PubMed: 19277971]
38. Claes A, Gambarota G, Hamans B, van Tellingen O, Wesseling P, Maass C, et al. Magnetic resonance imaging-based detection of glial brain tumors in mice after antiangiogenic treatment. Int J Cancer 2008;122:1981–6. [PubMed: 18081012]
39. Candolfi M, Curtin JF, Nichols WS, Muhammad AG, King GD, Pluhar GE, et al. Intracranial glioblastoma models in preclinical neuro-oncology: neuropathological characterization and tumor progression. J Neurooncol 2007;85:133–48. [PubMed: 17874037]
40. Gallo JM, Li S, Guo P, Reed K, Ma J. The effect of P-glycoprotein on paclitaxel brain and brain tumor distribution in mice. Cancer Res 2003;63:5114–7. [PubMed: 12941842]
41. Maria BL, Gupta N, Gilg AG, Abdel-Wahab M, Leonard AP, Slomiany M, et al. Targeting hyaluronan interactions in spinal cord astrocytomas and diffuse pontine gliomas. J Child Neurol 2008;23:1214–20. [PubMed: 18952588]
42. Gounder MK, Nazar AS, Saleem A, Pungaliya P, Kulkarni D, Versace R, et al. Effects of drug efflux proteins and topoisomerase I mutations on the camptothecin analogue gimatecan. Invest New Drugs 2008;26:205–13. [PubMed: 17943230]
43. Wang S, Zhou Q, Gallo JM. Demonstration of the equivalent pharmacokinetic/pharmacodynamic dosing strategy in a multiple-dose study of gefitinib. Mol Cancer Ther 2009;8:1438–47. [PubMed: 19509243]
44. Hofer S, Frei K. Gefitinib concentrations in human glioblastoma tissue. J Neurooncol 2007;82:175–6. [PubMed: 17008949]
45. Dukic SF, Heurtaux T, Kaltenbach ML, Hoizey G, Lallemand A, Vistelle R. Influence of schedule of administration on methotrexate penetration in brain tumours. Eur J Cancer 2000;36:1578–84. [PubMed: 10930807]
46. Blakeley JO, Olson J, Grossman SA, He X, Weingart J, Supko JG. Effect of blood brain barrier permeability in recurrent high grade gliomas on the intratumoral pharmacokinetics of methotrexate: a microdialysis study. J Neurooncol 2009;91:51–8. [PubMed: 18787762]
47. Ma J, Pulfer S, Li S, Chu J, Reed K, Gallo JM. Pharmacodynamic-mediated reduction of temozolomide tumor concentrations by the angiogenesis inhibitor TNP-470. Cancer Res 2001;61:5491–8. [PubMed: 11454697]
48. Langer O, Karch R, Muller U, Dobrozemsky G, Abrahim A, Zeitlinger M, et al. Combined PET and microdialysis for in vivo assessment of intracellular drug pharmacokinetics in humans. J Nucl Med 2005;46:1835–41. [PubMed: 16269597]
49. Vredenburgh JJ, Desjardins A, Herndon JE 2nd, Marcello J, Reardon DA, Quinn JA, et al. Bevacizumab plus irinotecan in recurrent glioblastoma multiforme. J Clin Oncol 2007;25:4722–9. [PubMed: 17947719]
50. Sorensen AG, Batchelor TT, Zhang WT, Chen PJ, Yeo P, Wang M, et al. A “vascular normalization index” as potential mechanistic biomarker to predict survival after a single dose of cediranib in recurrent glioblastoma patients. Cancer Res 2009;69:5296–300. [PubMed: 19549889]

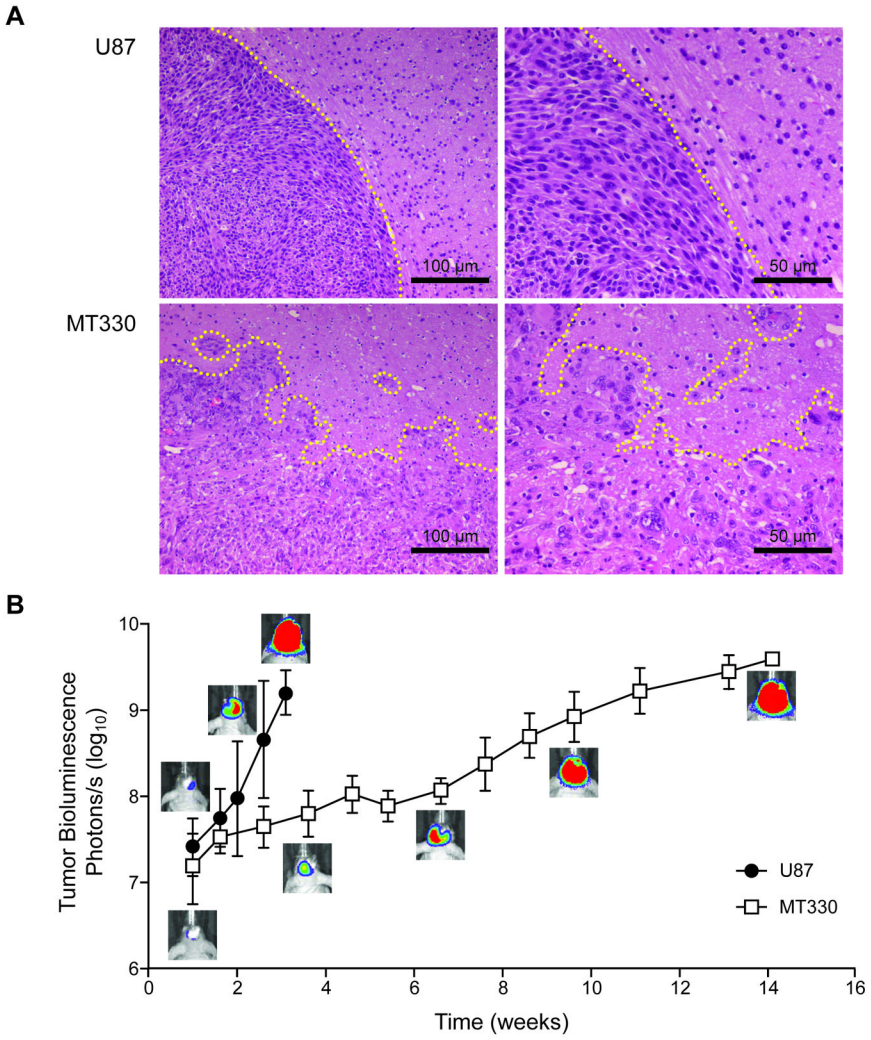


**Figure 1.**

Morphology and growth of U87 and MT330 tumor models. *A*, Histologic appearance of the xenografts (hematoxylin-eosin stain). Dotted yellow lines indicate the tumor margin. *B*, Tumor bioluminescence signal *versus* time. Mean ± SD of 5-15 values and representative bioluminescence pictures are shown.

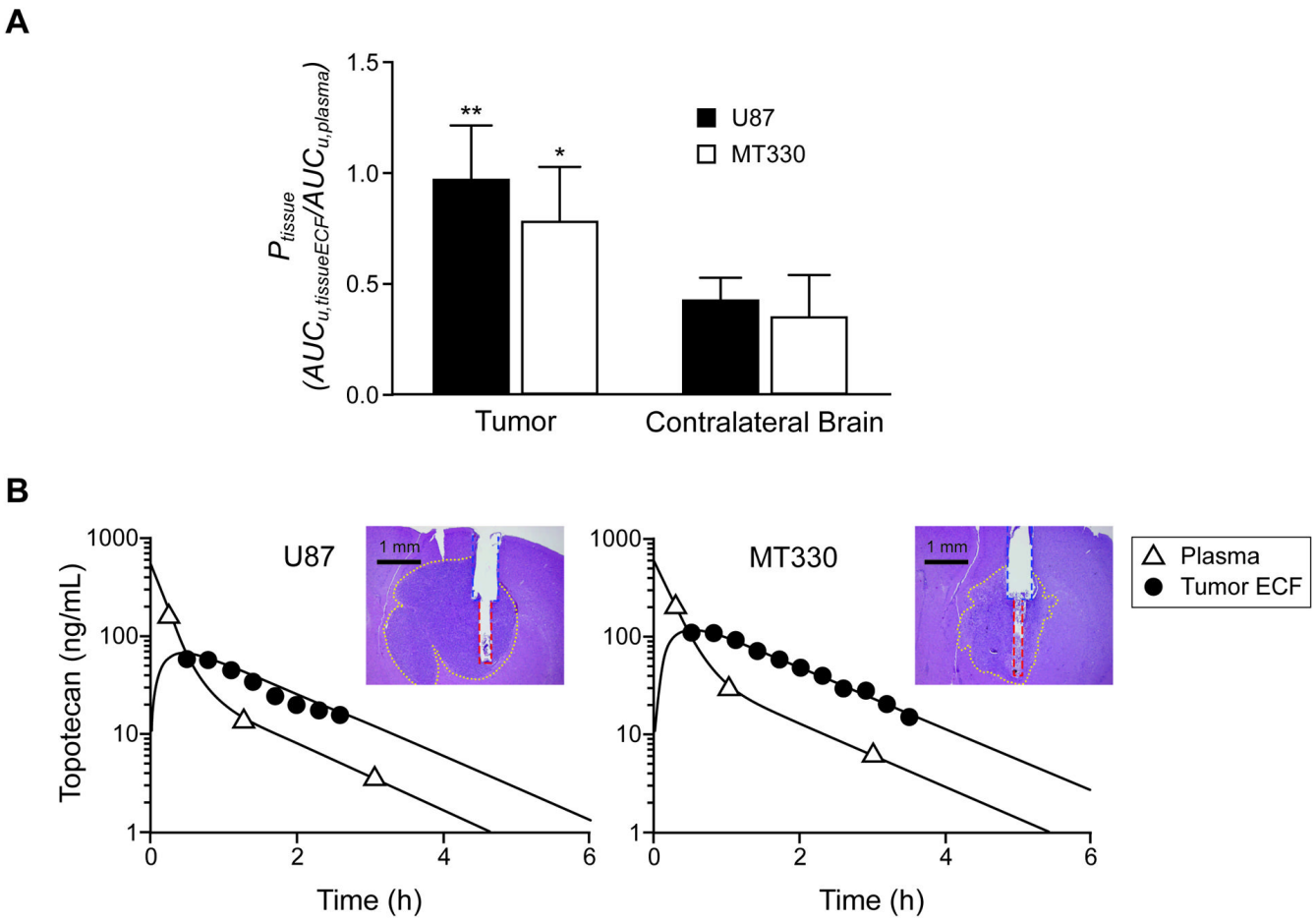


**Figure 2.**

Topotecan penetration of tumor and contralateral brain ECF after a 4-mg/kg i.v. dose in U87 and MT330 models. *A*, Comparison of $P_{tissue}$ means (SD), calculated as $AUC_{u,tissueECF}/AUC_{u,plasma}$ topotecan ratios in *tumor* and in *contralateral brain* tissue. **P = 0.001; *P = 0.013; *t* test, as compared to contralateral brain. *B*, Representative concentration-time graphs (experimental data and model-fitted curves) of topotecan (unbound lactone) in tECF and plasma. Histologic images confirming probe location are shown (yellow dots limit tumor margins, blue dashes limit cannula track, and red dashes limit probe track; lines were drawn with Adobe Photoshop V11.0).

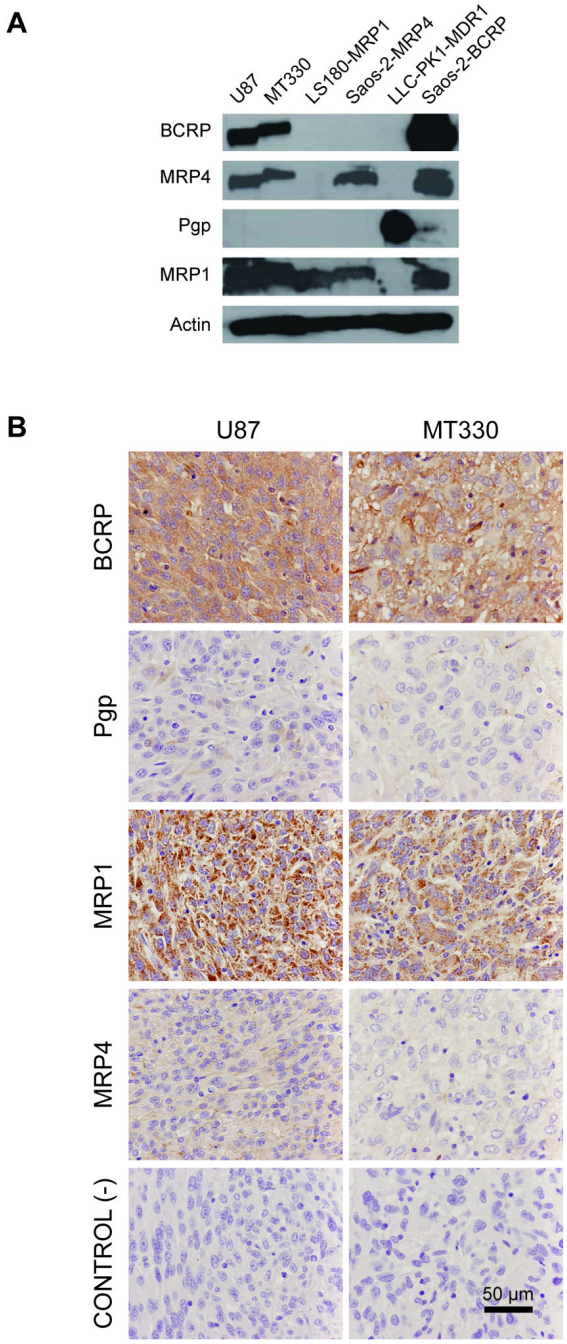


**Figure 3.**
Expression of ABC transporters in U87 and MT330 tumor models. *A*, Western blots of cells cultured *in vitro*. *B*, Immunostaining of tumor xenografts. Negative controls (tissue slides incubated with nonspecific rat IgG) are shown for comparison.

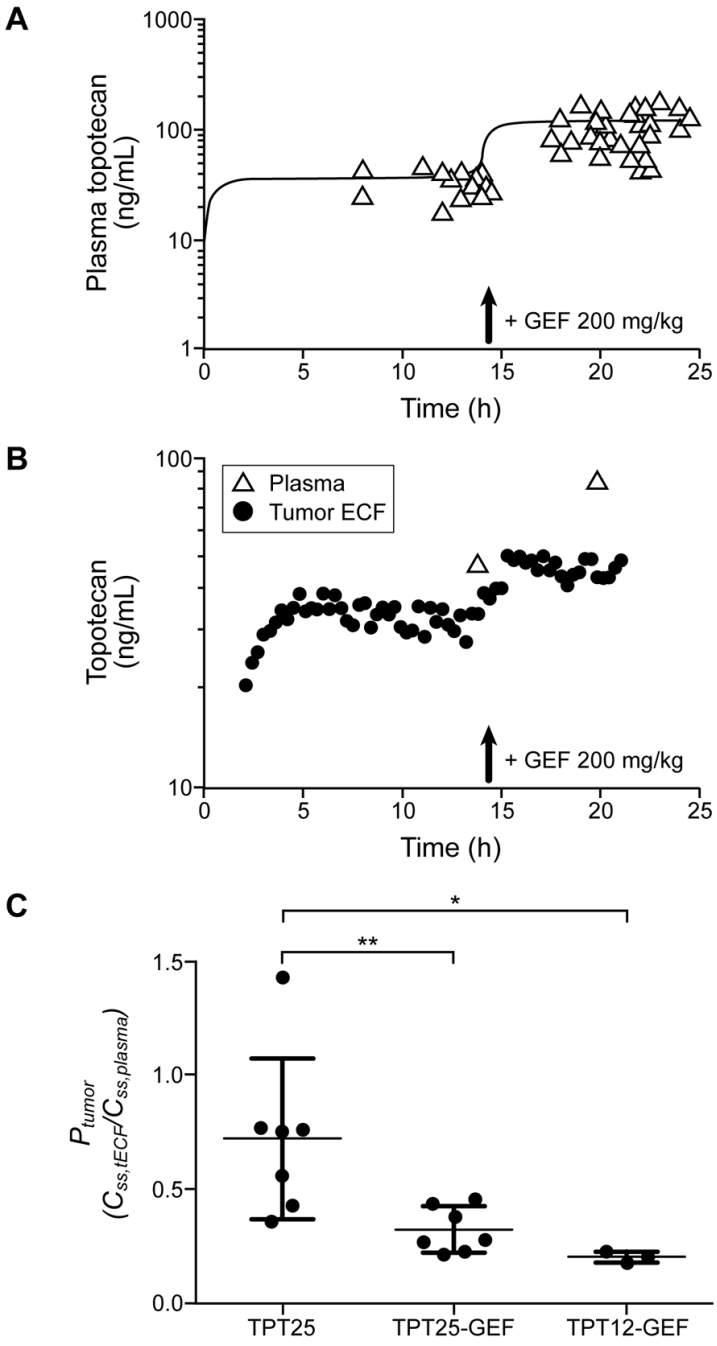


**Figure 4.**

Effect of gefitinib on topotecan ECF concentration in U87 tumors at the steady-state. *A*, Plasma concentration-time profile of topotecan (unbound lactone) in U87 tumor-bearing mice after insertion of pumps releasing 25 μg topotecan/h and before and after an oral dose of gefitinib (200 mg/kg, 14 h after pump insertion) (n=22; 1-4 plasma samples obtained from each; individual data and model-fitted curve are shown). *B*, Representative microdialysis data from a U87 tumor-bearing mouse implanted with a pump releasing 25 μg topotecan/h. Topotecan (unbound lactone) concentration in tECF dialysate and plasma are shown before and after administration of gefitinib (200 mg/kg) at 14 h. *C*, Tumor penetration ($P_{tumor}$), as $C_{ss,tECF}/C_{ss,plasma}$ ratios calculated from microdialysis-derived tECF and plasma topotecan (unbound

lactone) concentrations at the steady-state in mice receiving 25 μg/h topotecan, before (TPT25) and after (TPT25-GEF) receiving gefitinib (200 mg/kg at h 14 of topotecan) and in a group (TPT12-GEF) receiving 12.5 μg/h topotecan and 200 mg/kg gefitinib 0.5 h before topotecan. Individual values and mean ± SD are shown. * P = 0.017, Mann-Whitney test; **P = 0.009 paired *t* test.

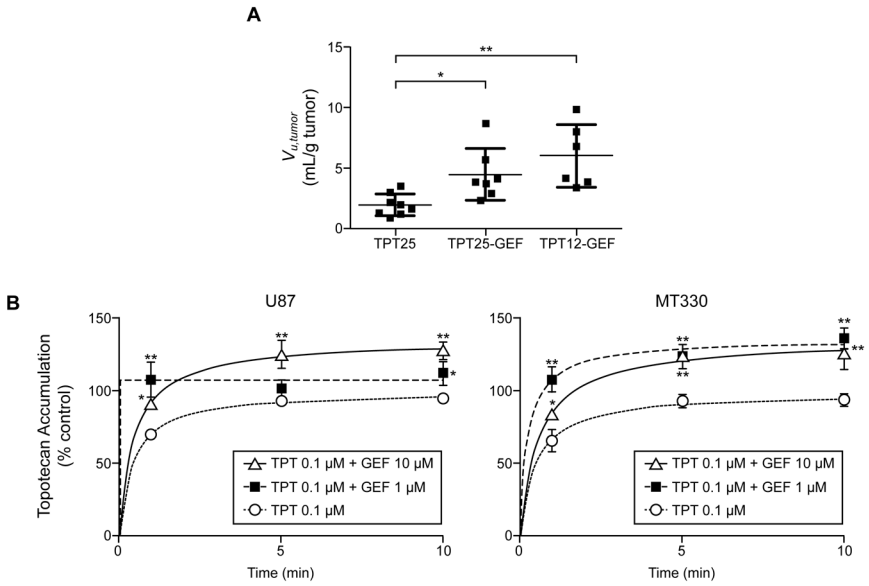


**Figure 5.**

Effect of gefitinib on topotecan accumulation in tumor xenografts *in vivo* and in tumor cells *in vitro*. *A*, $V_{u,tumor}$ values at steady-state in U87 tumors from mice receiving topotecan 25 μg/h (TPT25), topotecan 25 μg/h and gefitinib 200 mg/kg (TPT25-GEF), or topotecan 12.5 μg/h and gefitinib 200 mg/kg (TPT12-GEF; plasma exposure equivalent to that in the TPT25 group). Individual values and mean ± SD are shown. *P = 0.044, **P = 0.002; one-way ANOVA, post-hoc *t*-test with Bonferroni correction. *B*, Topotecan accumulation in tumor cells *in vitro* in the presence and absence of gefitinib. Values are the percentage of the maximum accumulation (mean ± SD; n=3) in control cells (topotecan 0.1 μM, no gefitinib) at each time point. *P < 0.05, **P < 0.01, as compared to accumulation in control cells at the same time point; one-way ANOVA, post-hoc *t*-test with Bonferroni correction.

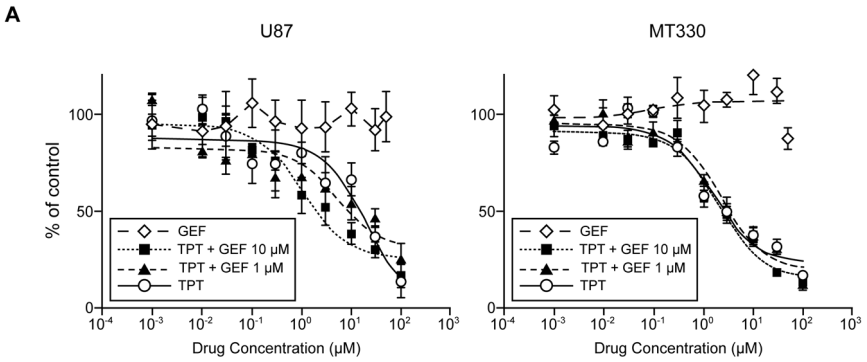


**Figure 6.**

Sensitivity of tumor cells to topotecan (TPT; 100-0.001 μM), gefitinib (GEF; 50-0.05 μM), and combinations of topotecan (100-0.001 μM) and gefitinib (1 and 10 μM). Values are the mean ± SD percentage of growth in untreated cells (n=5).